SECOND EUROPEAN CONFERENCE ON EARTHQUAKE ENGINEERING
AND SEISMOLOGY, ISTANBUL AUG. 25-29, 2014

SURFACE DEFORMATION TROUGHS INDUCED BY NORMAL FAULTING AND REVERSE FAULTING

Chung-Jung LEE[1], Yu-Yi CHANG[2], and Wen-Yi HUNG[3]

ABSTRACT

A series of centrifuge normal faulting and reverse faulting tests was conducted at different *g*-levels to investigate the effect of the vertical throw in the extents and in the magnitudes of surface deformation profile at various vertical throws. The faulting events that is simulated at high *g*-levels can effectively reduce the errors resulted from the capillarity force and give the more real results of the surface deformation profiles. The measured surface deformation profiles at various vertical throws gives the possible influence zones induced by normal and reverse faulting. The influence zone caused by normal faulting with a 60^o dip angle is about 0.8 times of the overburden soil thickness and that induced by reverse faulting with a 60^o dip angle is about 1.0 times of the overburden soil thickness. The thicker the overburden soil deposit is, the wider influence zone is observed.

INTRODUCTION

Large scale earthquakes would cause large surface deformation as a result of uplifting or falling of the overburden soils due to normal or reverse faulting and definitely cause severe damages to buildings, infrastructures, and lifelines located within the zone of faulting. Figure 1 shows the surface deformation induced by reverse faulting after the 921Taiwan Chi-Chi Earthquake in the playground of Kung-Fu junior high School [http://www.921emt.edu.tw]. This behavior has been highlighted in the recent inland earthquakes in Turkey, Japan, Iran, and China. In general, the surface displacements induced by normal or reverse faulting can be divided into two components: vertical uplift (or falling) and lateral offset at the ground surface. Man-made structures or piping utilities in close proximity to a rupture zone on the ground surface or embedded in the subsurface distortion zone can suffer severe damages as shown in Figure 2.

The extent of surface deformation trough and setback distance from an active fault is the most essential issues for the disaster preventions in the nation land and urban planning [Bransby et al. 2008; Bransby et al. 2008]. There have been many researches, use of fielding investigation involving trench, numerical modeling and/or physical experiments to investigate the development of surface deformation trough and subsurface distortion zone . Physical modeling consists of two types of experiments, 1-*g* and centrifuge modeling. In the study, a series of centrifuge normal and reversal faulting tests was performed to investigate the effect of the vertical throw (h) in the extent and magnitude of surface deformation trough. The normal and reverse faults of dip angle of 60^o (at bedrock level) were initiated through the overburden sand layer and emerged on the ground surface. The surface deformation profiles at various vertical throws were recorded and analyzed.

[1] Professor, Dept. of Civil Engineering, National Central University, Jhongli, Taiwan, cjleeciv@ncu.edu.tw
[2] Dr., Dept. of Civil Engineering, National Central University, Jhongli, Taiwan, 93342004@ncu.edu.tw
[3] Assistant Professor, Dept. of Civil Engineering, National Central University, Jhongli, wyhung@ncu.edu.tw

Figure 1. Surface deformation trough after the Chi-Chi Earthquake (http://tw.myblog.yahoo.com)

Figure 2. Damages of Building caused by the reverse faulting in the 1991 Chi-Chi Earthquake

TESTING FACILITIES AND SETUP AND TESTING PROCEDURES

This experimental work was undertaken in the geotechnical Centrifuge at the National Central University (NCU). The NCU Geotechnical Centrifuge has a nominal radius of 3 m and equips a 1-D servo-hydraulically controlled shaker integrated into a swing basket and tested at a maximum acceleration of 80 g [Lee et al. 2012].

A fault simulation container with an acrylic window of 60 cm × 28.15 cm is designed to conform to the constraints on the space and load capacity of the platform in the NCU centrifuge. The dimensions of the fault simulation container are 100 cm×52.8 cm×67.5 cm (length×width×height) as shown in Figure 3 and Figure 4. An AC-220V-200W motor and a 1/200 gear box reducer is installed in the container, a remote adjustable speed meter is setup in the control panel. The container can simulate the normal/reverse fault slip and adjust the slip speed from 0~2.5 mm/min. The maximum vertical slip (uplift and falling height) can reaches 5.5 cm. The spaces of 74 cm in length, 32.9 cm in width, and 30 cm in height was provided for the soil bed in the container. A L-shape push panel having the dimensions of 15 cm x 30 cm x 25 cm is manufactured to push the tested soil bed upward (reverse faulting) or to move the tested soil bed downward (normal faulting) with a dip angle of 60^o through the soil layer. This mechanism gives the opportunity to perform the normal and reverse fault tests. An in-flight surface profile scanner equipped with two laser displacement transducers installed horizontally and vertically and driven with a motor with a sampling rate of 100 samples/sec can densely scanned the surface elevations on the center line of the tested sand bed during faulting tests. An acrylic window

of 60 cm×28.15 cm as shown in Figure 3 was used to observe the deformation patterns of subsurface during normal faulting and reverse faulting.

A quartz sand was used to prepare the uniform sand bed for all the tests in the study. The fine uniform silica sand with D_{50}=0.193 mm, ρ_{max} =1660kg/m^3, ρ_{min} = 1380 kg/m^3, and with peak friction angle $\emptyset_{peak}$=38^o, and dilation angle, φ'=6^o was measured for D_r=70% at the normal stress = 200 kPa. The dry quartz sand was pluviated with a regular path into the container from a hopper at a specified falling height and at a constant flow rate for preparing fairly uniform sand deposits having relative density of around 70%. The pluviation process was interrupted as needed for spraying a thin layer of blue dyed sand at specified elevations as marker layers in close proximity to the acrylic window to allow identification of shear deformation in the subsurface. The sand bed of 20 cm thick was prepared (corresponding to 16 m at prototype scale when tested at the 80 *g* of acceleration).

After completing the centrifuge flight safety checks the centrifuge was accelerated at an acceleration of 10 *g* per step until it reached the target acceleration or the acceleration of 80 *g*. In each step the surface profile scanner was trigged to scan the surface of soil bed for measuring the changes in the surface elevations. Once the centrifuge reached the target acceleration (40 *g* or 80 *g*), normal and reverse faulting was conducted. The normal faulting was actuated with the L-shape panel moving downward along the dip angle of 60^o. The reverse faulting was actuated with the L-shape panel moving upward along the dip angle of 60^o. Figure 4 shows the dimensions of the fault simulation container and the coordinate system used to demonstrate the testing results of normal fault test and reverse fault test, as discussed in the following sections. As shown in Figure 5, the origin of the coordinate system was the point at which the fault tip vertically projected onto the ground surface for normal and reverse faulting. The fault throw was increased (reverse faulting) or decreased (normal faulting) at a constant velocity of 2 mm/min using an AC motor. The surface profile scanner was driven once to scan the surface elevations per 2.5 mm vertical throw increment. The ratio of the vertical throw (*h*) to the overburden soil thickness (*H*), *r* (%), is defined as:

$$r\ (\%) = \frac{h}{H} \times 100 \qquad (1)$$

The fault slip displacement increased until reaching a final throw of 50 mm (*r* = 25%, corresponding to a vertical throw of 4 m at the prototype scale at the acceleration of 80 *g*). In total, 20 scans were performed (S1–S20; *r* = 1.25% – 25%) to measure the evolution of the ground surface profile during the normal fault and reverse fault tests.

The testing program is listed in Table 1. A total of 8 tests those which were divided into two groups were performed. One is the normal faulting test (80*g*Ntest#) and the other is reverse faulting test (80*g*Rtest#). Here "80g" represents the testing *g*-level is 80 *g*. In the study the normal faulting tests and the reverse faulting tests were performed at the acceleration of 1 *g*, 40 *g* and 80 *g*. The symbol "Ntest#" is referred to the normal faulting test, and "Rtest#" is referred to the reverse faulting test. "#" is the test number.

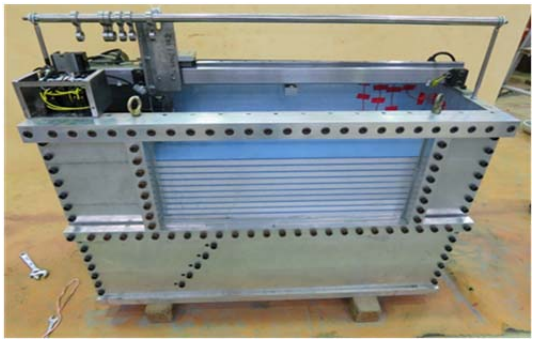

Figure 3. The fault simulation container

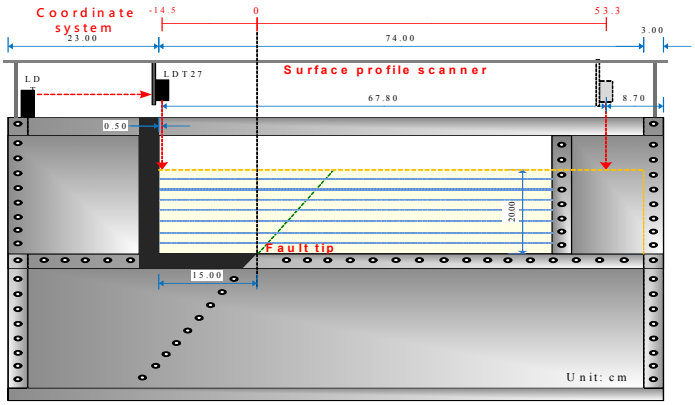

Figure 4. Dimensions of the fault simulation container and the coordinate system

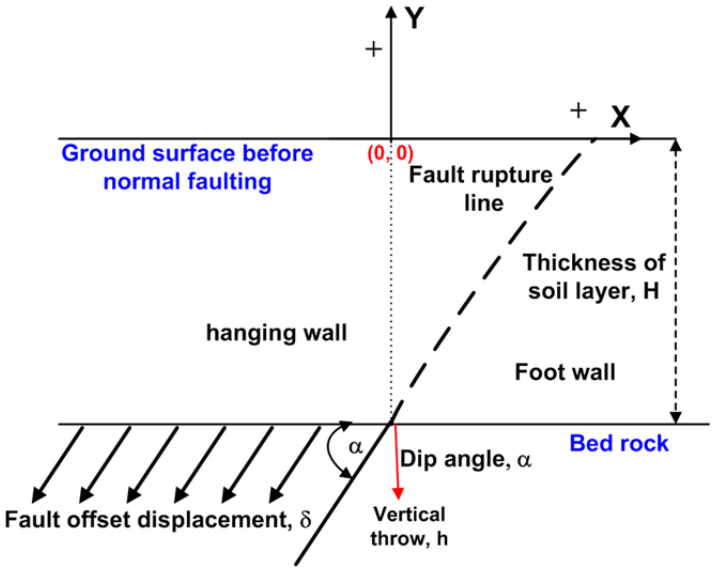

(a) Normal fault

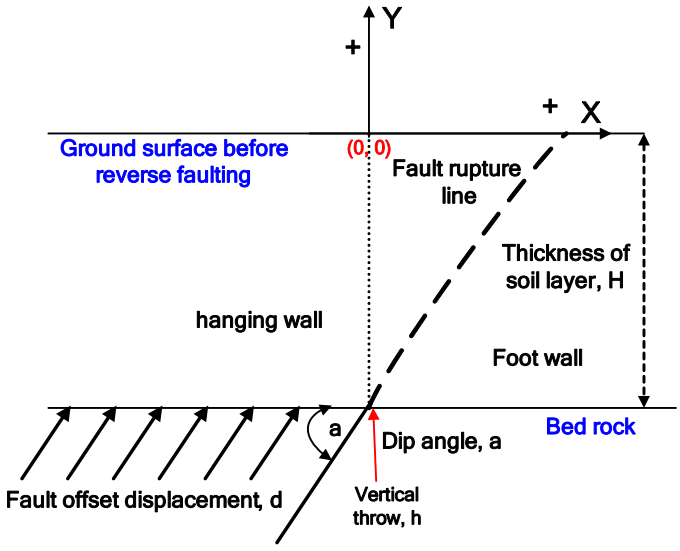

(b) Reverse fault

Figure 5. Definition of the coordinate system and the geometry of overburden soil layer and the fault tip of the fault: (a) Normal fault; (b) Reverse fault

Table 1. Testing conditions in the study

Normal faulting test				Reverse faulting test			
Test No.	D_r (%)	*Thickness of overburden (cm)	*vertical throw (cm)	Test No.	D_r (%)	*Thickness of overburden (cm)	*Vertical throw (cm)
80gNtest28	70	20 (16 m)	-5 (4 m)	80gRtest22	70	20 (16 m)	5 (4 m)
80gNtest29	70	20 (16 m)	-5 (4 m)	80gRtest23	70	20 (16 m)	5 (4 m)
40gNtest30	70	20 (8 m)	-5 (2 m)	40gRtest17	70	20 (8 m)	5 (2 m)
1gNtest31	70	20 (0.2 m)	-5 (0.05m)	1gRtest18	70	20 (0.2 m)	5 (0.05m)

*Model dimensions are in centimeter and prototype dimensions (in parentheses) are in meters.

TEST RESULTS AND INTERPRETATIONS

This article focuses on the surface and subsurface deformation profiles induced by normal and reverse faulting along a 60° dip angle. The geometry of the overburden soil layer and the normal and reverse faults is shown in Figure 5(a) and Figure 5(b). The origin of the coordinates in the X-axis is set at the position of fault tip and that in the Y-Axis is at the ground surface before faulting. The vertical throw, *h*, is obtained from the uplift or falling height of L-shape panel. Based on this coordination system the surface deformation profiles measured at various vertical throws by means of the profile scanner can be plotted.

Surface and Subsurface Deformation Profiles Induced By Normal Faulting

The normal faulting was actuated with the L-shape panel moving downward along the dip angle of 60°. The progressive rupture failure was observed as the increase of downward vertical throw, *h*. Figure 6 shows the surface deformation profiles at various throws for 80*g*Ntest29. The Y-axis in Figure 6(a) represents the magnitude of falling height (negative value) on the surface induced by normal faulting. The Y-axis in Figure 6(b) represents the changes in the elevations of ground surface at various throws during normal faulting. The thickness of overburden soil layer, *H*, is 20 cm in model scale and is the thickness of 16 m in prototype scale. The inclined line in Figure 6(b) displays the normal faulting is downward falling along the slip dip angle of 60°. The maximum downward vertical throw was -5 cm. The surface deformation profiles were measured per vertical throw of 2.5 mm, *h*. There were totally 20 measured surface deformation profiles (S1 – S20) in each test.

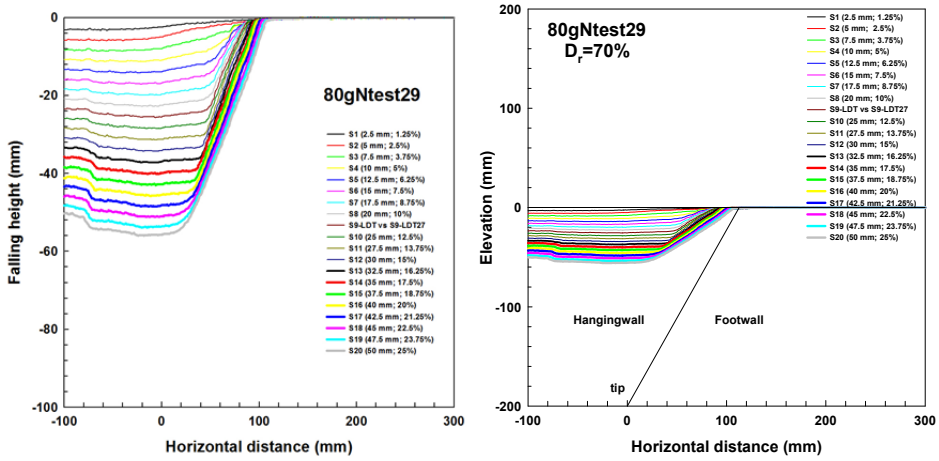

(a) (b)

Figure 6. Surface deformation profiles at various throws for normal faulting (80gNtest29): (a) detailed surface deformation; (b) the relation between the surface deformation profiles and the fault tip (Both dimensions in model scale)

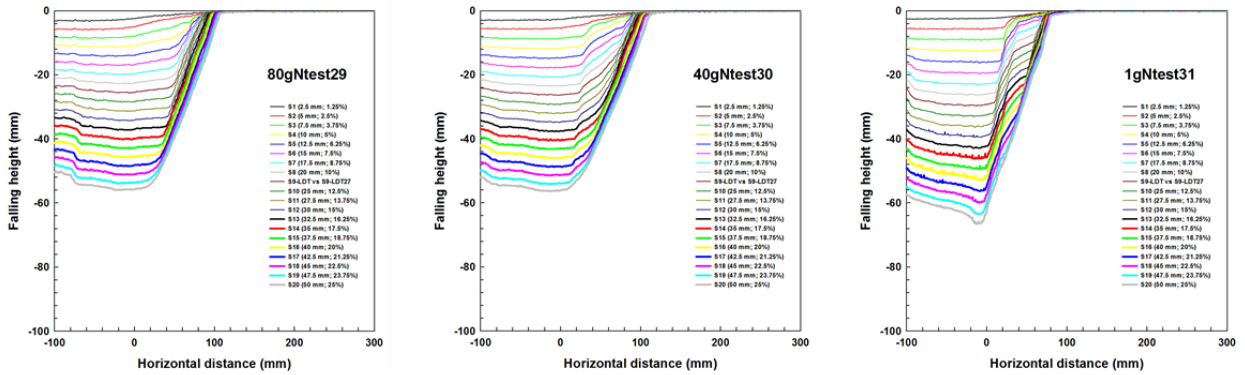

(a) (b) (c)

Figure 7. Comparison of surface deformation profiles tested at different *g*-levels for normal faulting: (a) 80 *g*; (b) 40 *g*; (c) 1 *g*.

As expected the falling height on the ground surface increases with the increases of the downward vertical throw. The maximum falling height occurs at around the horizontal distance of 0 (at the original position of fault tip) and the value of maximum falling height is 10% larger than the corresponding vertical throw (5 cm). The surface deformation profile starts from the point on the ground surface which is about located at the 60^{o} fault slip line. Figure 7 shows the comparison of the surface deformation profiles tested at 1 *g*, 40 *g*, and 80 *g*. The surface deformation profiles obtained from the tests of high-*g* level are similar but those which obtained from the 1 *g* test have the larger falling height and the steeper surface slopes because of the existence of capillarity forces among the sand particle.

Figures 8(a)- 8(c) show photos of the subsurface deformation profiles which are taken from the acrylic window after the normal faulting tests (h = -5 cm) at the accelerations of 1 *g*, 40 *g*, and 80 *g*, respectively. The 10 thin-colored sand marked layers in the soil bed provide a better visual identification of the rupture pattern after normal faulting. The soil mass with the higher confining pressure has the smaller dilation angle. Because the 80*g*Ntest24 has the smallest dilation angle, therefore, the location of the upper-bound rupture of 80*g*Ntest24 is on the most right hand side. Furthermore, because of the lowest dilation angle in the model scale of 80*g*Ntest24 the shear strength of the soil mass is the smallest and then it makes the flattest slope on the escarpment of 80*g*Ntest24 as a result of the more volume of sand mass moves into the escarpment. In contrast there is the deepest depth of escarpment if the model is tested in 1 *g* condition because the less volume of sand mass fall into the space

(a) 80*g*Ntest24

(b) 40*g*Ntest26

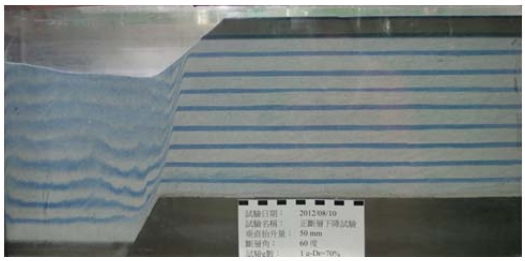

(c) 1*g*Ntest31

Figure 8. Photos of subsurface deformation patterns tested at different g-levels after 5-cm-throw normal faulting tested at: (a) 80 *g*; (b) 40 *g*; (c) 1 *g*.

Surface deformation Profiles Induced by Reverse Faulting

The reverse faulting was actuated with the L-shape panel moving upward along the dip angle of 60°. The progressive rupture failure was observed as the increase of vertical throw, *h* (positive value). Figure 9 shows the surface deformation profiles at various throws. The same coordinate system as described in the normal faulting tests was used to plot the surface deformation profiles except that the positive vertical throw represents the upward movement. The thickness of overburden soil layer, *H*, is 20 cm in model scale and is the thickness of 16 m in prototype if tested at the acceleration of 80 *g*. The inclined line in Figure 9(b) also points the reverse faulting is upward rising along the slip dip angle of 60°. The maximum vertical throw was +5 cm. The surface deformation profiles were measured per vertical throw of 2.5 mm, *h*. There were totally 20 measured surface deformation profiles (S1 – S20) in each test.

Figure 10(a) shows the surface deformation profiles at various *r*(%) those which range from 1.25% to 25%. The relative density of this tested bed is 70%. As expected the uplifting height increases with the increase of the vertical throw. The maximum uplifting height occurs at around the horizontal distance of 0 (at the position of fault tip) and the value of maximum uplifting height is 10% larger than the corresponding vertical throw. The surface deformation profile starts from the point which is about located at the 60° fault slip line as shown in Figure 10(b). Figure 10 shows the comparison of the surface deformation profiles tested at 1 *g*, 40 *g*, and 80 *g*. The surface deformation profiles obtained from the tests of high-*g* level did not show obvious different patterns but those profiles obtained from 1 *g* tests has the steeper surface slopes because of the existence of capillarity forces among the sand particle to increase the effective stresses in the soil mass and tthe larger dilation angle is expected in the lower confining pressure.

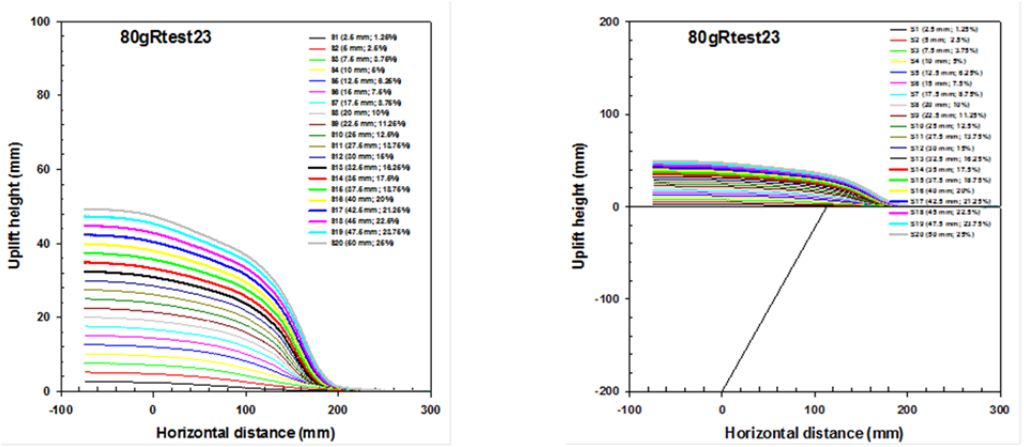

(a) (b)

Figure 9. Surface deformation profiles at various throws for reverse faulting (80*g*Rtest23): (a) detailed surface deformation; (b) the relation between the surface deformation profiles and the fault tip (Both dimensions in model scale)

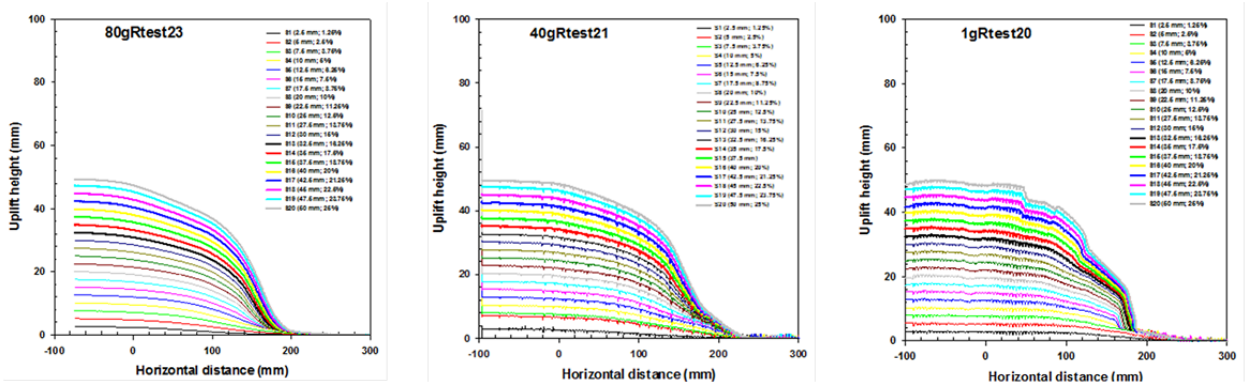

Figure 10. Comparison of surface deformation profiles tested at different g-levels for reverse faulting: (a) 80 *g*; (b) 40 *g*; (c) 1 *g*.

Figures 11(a)- 11(c) show photos of the subsurface deformation profiles which are taken from the acrylic window after the reverse faulting tests (h = 5 cm) at the accelerations of 1 *g*, 40 *g*, and 80 *g*, respectively. After examining the subsurface deformation patterns in the shallower depths as shown in Figs 11(a)-11(b), we found that more faulting lines were developed in the 1-*g* reverse faulting test than that in the higher *g* reverse faulting tests. The major faulting-induced distortion zones appeared in the sand beds, when tested at 1 *g*, 40 *g*, and 80 *g*, differ significantly. The distorted zone induced by the reverse faulting tested at 80 *g* has the narrowest width of shear band, whereas that induced by the reverse faulting tested at 1 *g* has the widest shear band width. The distorted zone induced by the reverse faulting tested at 40 *g* lies in between. These results might be caused by following two possible mechanisms: (1) the small capillarity forces developed between the sand particles (apparent cohesion), which increases the effective stresses in the soil mass. (2) higher rate of dilation occurred when the soil mass was sheared in the lower confined stress (tested at the lower *g* level or in the shallower depth of sand bed). Centrifuge reverse faulting tests can more precisely simulate in-situ stress levels, and are absolutely necessary for investigating the field reverse fault mechanism.

(a) 80 *g*

(b) 40 *g*

(c) 1 *g*

Figure 11. Photos of subsurface deformation patterns tested at different g-levels after 5-cm-throw normal faulting tested at: (a) 80 *g*; (b) 40 *g*; (c) 1 *g*.

CONCLUSIONS

Use of the centrifuge fault simulation container the events of normal and reverse faulting with a 60^{o} dip angle were modeled at the accelerations of 1*g*, 40*g*, and 80 *g*. The faulting event simulated at the high *g*-levels can effectively reduce the errors resulted from the capillarity force and give the more real results of the surface deformation profiles. The surface deformation profiles have steeper surface slopes in the 1-*g* reverse faulting model test than those tested at higher *g* levels. The observed subsurface rupture pattern shows more faulting in the shallower depths in the 1-*g* test than those observed in the higher *g* tests. The observed major faulting-induced distortion zone on the higher *g* model test also has a narrower shear band width. This may be because the small capillarity force developing among the sand particles increases the effective stresses in the soil mass, and a higher rate of dilation that occurs if the soil mass is tested at the 1 *g* level or in the shallower depths. The measured surface deformation profiles at various vertical throws gives the possible influence zone induced by normal and reverse faulting. The influence zone caused by normal faulting with a 60 ^{o} dip angle is about 0.8 times of the overburden soil thickness and that induced by reverse faulting with a 60 ^{o} dip angle is about 1.0 times of the overburden soil thickness. The thicker the overburden soil deposit the wider influence zone is observed.

REFERENCES

Bransby, M.F., Davies, M.C.R., and El Nash, A. (2008), "Centrifuge Modeling of Reverse Fault-foundation Interaction," *Bulletin of Earthquake Engineering*, Vol.6, pp.607-628.

Bransby, M.F., Davies, M.C.R., and El Nash, A. (2008), "Centrifuge Modeling of Normal Ffault-foundation Interaction," *Bulletin of Earthquake Engineerin*g, Vol.6, pp.585-605.

Lee, C.J., Wang, C.R., Wei, Y.C. Hung, W.Y. (2012), " Evolution of the Shear Wave Velocity During Shaking Modeled in Centrifuge Shaking Table Tests," *Bulletin of Earthquake Engineering*, Vol.10, No.2, pp.401-420.

921 Earthquake Museum of Taiwan: http://www.921emt.edu.tw.